

## Mechanical Properties of 17-4 PH Stainless Steel Additively Manufactured under Ar and N<sub>2</sub> Shielding Gas

Pooriya Dastranjy Nezhadfar<sup>1,2</sup>, Mohammad Masoomi<sup>1,2</sup>, Scott Thompson<sup>1,2</sup>, Nam Phan<sup>3</sup>, Nima Shamsaei<sup>1,2\*</sup>

<sup>1</sup> Department of Mechanical Engineering, Auburn University, Auburn, AL, 36849

<sup>2</sup> National Center for Additive Manufacturing Excellence (NCAME), Auburn University, AL, 36849

<sup>3</sup> Structures Division, U.S. Naval Air Systems Command, Patuxent River, MD 20670

\*Corresponding author: [shamsaei@auburn.edu](mailto:shamsaei@auburn.edu)

### **Abstract**

This study investigates the effect of using either argon or nitrogen as the shielding gas on the final mechanical properties of additively manufactured (AM) 17-4 PH stainless steel (SS). The difference in thermo-physical properties of shielding gases during the additive manufacturing process can affect part thermal response. Simulations are performed to elucidate the differences in temperature, temperature gradient and cooling rate for argon and nitrogen building environments for the laser-powder bed fusion (L-PBF) process. Mechanical properties of fabricated parts are studied through micro-hardness and tensile tests. Tensile tests are carried out under 0.001 s<sup>-1</sup> strain rate at room temperature. Using both numerical and experimental results, the effects of shielding gas type on AM 17-4 PH SS will be presented and discussed.

**Keywords:** Tensile properties; Micro-hardness; Shielding gas; Thermal simulation; 17-4 PH stainless steel; Laser powder bed fusion

### **Introduction**

Additive manufacturing (AM) is a novel manufacturing method which provides more freedom in design, manufacturing near net shaped parts per demand, lower cost of production and expedition in delivery time to market [1]. Recently, AM has drawn attention from academia and industry with the aim of fabricating high-quality parts with optimal mechanical performance. AM can be classified to various techniques such as laser powder bed fusion (L-PBF), direct laser deposition (DLD), binder jetting, and ultrasonic additive manufacturing (UAM), based on the energy source, feed stock and feeding system. Among various metals AM techniques, L-PBF is the most prominent one and provides higher accuracy and powder proficiency in comparison to other methods. During the L-PBF process, a thin layer of metallic powder is spread by a recoater arm and fused to the previous layer via the laser heat flux in an inert atmosphere. This process occurs repetitively, until the part is completed.

Beside the benefits of AM methods, there are some drawbacks to AM parts, as they can consist of defects such as pores and lack of fusion (LOF) which are inherited from the process.

Accordingly, the trustworthiness of the fabricated parts must be investigated prior to using them in critical load bearing applications. Many efforts have been done to optimize or improve the mechanical properties of AM parts by investigating various process parameters, scan strategies and building orientation effects [2-4]. Shielding gas has been introduced as another significant parameter which affects not only the thermo-physical but also the mechanical properties of fabricated parts [5]. The shielding gas is responsible for the removal of reactive gases surrounding the melt pool to prevent detrimental effects of reaction with atmospheric gases like oxygen [6]. Various factors such as the base material and chemical-metallurgical reactions of the gas with the melt pool must be considered for choosing the appropriate shielding gas [7]. Effects of various shielding gases such as argon, nitrogen and helium have been studied on the behavior of different materials (e.g. carbon steels, stainless steels, aluminum alloys) [6, 8, 9]. In addition, several numerical simulation studies have been conducted to investigate shielding gas effects on the behavior of materials. Zekovic et al. [10] modeled convection in vicinity of the melt pool using computational fluid dynamics (CFD) for the direct laser metal deposition (DMD) of H13 tool steel. It was found that modeling the DMD gas flow better estimates convection heat transfer, resulting in more accurate residual stress modeling. In some cases, radiation and convection have been assumed as negligible during L-PBF [11, 12] while others have assigned a uniform/constant heat transfer coefficient over all free surfaces. Heigel et al. [13] modeled convection using a measurement-based method for DMD of Ti-6Al-4V. It was shown that using a more accurate heat transfer coefficient can reduce the error in temperature prediction by up to 30%.

17-4 precipitation hardening (PH) stainless steel (SS) is a martensitic precipitation hardenable SS which has been drawn into attention recently for use in AM. 17-4 PH SS is well known for its high tensile/impact strength, fracture toughness and corrosion resistance at service temperatures below 300 °C and is thus used as the structural material in aerospace, petrochemical, power plants and marine environments [14]. The phase composition of AM 17-4 PH SS has been investigated in argon and nitrogen building environments. Nitrogen has been shown to stabilize the austenite and affect the precipitation behavior in further heat treatment which is influential on the mechanical properties as compared to the argon building environment [15].

To the best of authors' knowledge, there is a significant gap in the literature regarding the effects of shielding gas type on the behavior of AM parts considering the different thermal properties of various gases. Accordingly, the current study focuses on modeling the thermal response of 17-4 PH SS by simulating a single track during typical L-PBF conditions while considering convection heat transfer for different shielding gases. The gas momentum and energy fields are found numerically while referencing temperature-dependent properties. Effects of convection and radiation heat transfer under different shielding gases (i.e. nitrogen and argon) on the temperature distribution, temperature gradient and local heating/cooling rates of 17-4 PH SS during L-PBF are investigated. The differences between simulating L-PBF with an assumed constant heat transfer coefficient versus locally-variable heat transfer coefficients, found via CFD of surrounding fluid flow in the chamber, are also elucidated. Experiments are performed to demonstrate and validate the effects of shielding gas type on the mechanical properties of L-PBF specimens.

### **Materials and methods**

Argon atomized 17-4 PH SS powder with particle sizes in the range of 15-45  $\mu\text{m}$  were provided by LPW Inc. for this study. The chemical composition of the powder is presented in [Table 1](#). Two sets of 11×11 mm square bars were vertically fabricated in two different building

environments, Ar (99.9997%) and N<sub>2</sub> (99.9997%), using EOS M290, an L-PBF system. The fabricated square bars were machined afterwards to the geometry based on the ASTM E606 [16]. Figure 1 provides a schematic of fabricated square bars and drawing of the final geometry of machined specimens. The process parameters employed for the fabrication of parts are shown in Table 2.

**Table 1.** Chemical composition of 17-4 PH stainless steel powder

	C	Cr	Ni	Cu	Mn	Si	Nb	Mo	N	O	Fe
(Wt. %)	0.01	15.6	4.03	3.89	0.24	0.29	0.33	<0.01	0.01	0.05	Bal

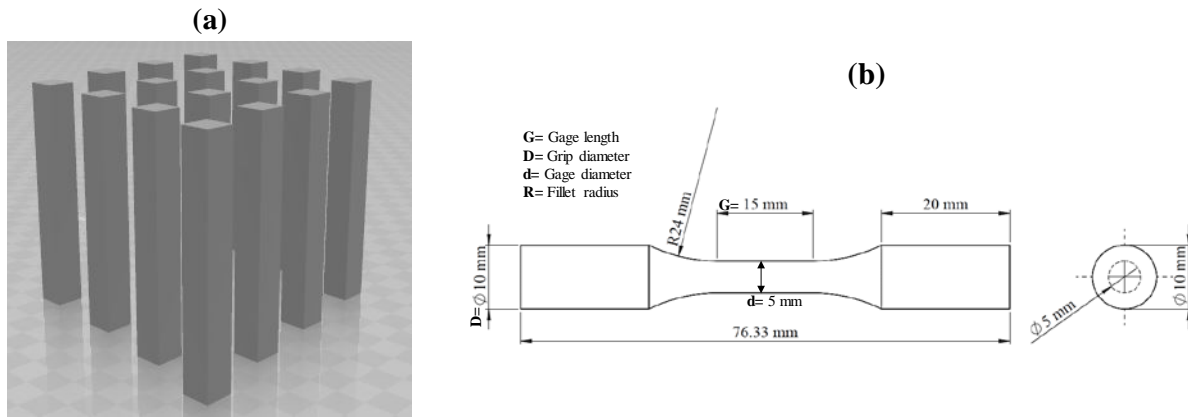


**Figure 1.** (a) 3D schematic of fabricated square bars, (b) the final geometry of machined specimens

The machined specimens were subjected to solution heat treatment for half an hour at 1050 °C, followed by air cooling to room temperature, and subsequent 4 hours annealing at 552 °C (CA-H1025 procedure) followed by air cooling to room temperature. Argon atmosphere was used during heat treatment to avoid oxidation. To remove the machining lines and dirt on the surface due to the heat treatment process, specimens were polished progressively to a mirror like surface finish. For better tracking each set in the following context, HT-Ar/Ar and HT-Ar/N<sub>2</sub> are the designations used for heat treated specimens that were built in Argon and Nitrogen atmosphere, respectively, and AB-Ar/Ar and AB-Ar/N<sub>2</sub> are the designations used for specimens in the as-built condition fabricated in Argon and Nitrogen, respectively. Micro Vickers Hardness (MVH) tests were carried out for all conditions employing DM 400 hardness tester equipment. Specimens were cross sectioned transversely in the gage section, progressively polished to mirror surface finish level and subjected to 100 gf loading with 10 s loading time for each indentation. In addition, Imagej software was used for quantifying the microstructural features (e.g. aspect ratio of the grains).

Additionally, specimens were subjected to uniaxial tensile tests at room temperature at 0.001 s<sup>-1</sup> strain rate using an MTS Landmark servo hydraulic test system with 100 kN load cells. Tests were carried out in two steps, strain-controlled and displacement controlled. Due to the

higher displacement of the material to the failure and the probability of extensometer destruction, the strain-controlled step was carried out using an extensometer up to 0.045 mm/mm strain, then continued in displacement control to the final fracture by removing the extensometer. For reducing uncertainty, three tensile tests were conducted for each condition and eventually the average values are presented.

### **Physical model and numerical method**

The validated numerical model was used for simulating the L-PBF of a single-track of 17-4 PH SS with a length of 5 mm. The size of the substrate and chamber size were 32 x 32 x 10 cm<sup>3</sup> and 25 x 25 x 35 cm<sup>3</sup>, respectively. Note that the area of the powder bed was smaller relative to the substrate. The five sides of the powder bed exposed to the gas were subjected to convection and radiation heat transfer. Process parameters used for simulation corresponding to recommended EOS M290 process parameters for fabricating dense 17-4 PH SS parts are presented in [Table 2](#).

**Table 2.** Process parameters for 17-4 PH stainless steel provided by EOS.

<b>Laser power (W)</b>	<b>Scanning speed (mm/s)</b>	<b>Hatching distance (<math>\mu\text{m}</math>)</b>	<b>Layer thickness (<math>\mu\text{m}</math>)</b>
220	755.5	100	40

The measurement, i.e. data extraction, location was at the middle of the track during the simulated fabrication. The simulation was repeated using different mesh sizes to ensure mesh-independent results. Results were reviewed to ensure that melt pool size was independent of mesh size. From the aforementioned simulations, melt pool length was found to become independent of mesh size when using 5000  $\mu\text{m}^3$  elements. Hence, simulations were performed using a mesh with element sizes of 3800  $\mu\text{m}^3$ . It should be noted that the thermal and velocity boundary layers in the chamber consisted of ~20 cells. Material property of 17-4 PH SS, argon and nitrogen gases used in the simulation were obtained from Masoomi et al. [17] and Younglove [18]. More details regarding the simulation conditions can be found in Ref [5].

## **Results and discussion**

### **Numerical study**

The unsteady momentum and energy transfer within the pumped/supplied argon/nitrogen gas, as well as the energy transfer within the irradiated powder bed and part during a typical L-PBF process, were predicted by solving their governing equations as defined for three-dimensional Cartesian space. To predict the convective heat flux between the build plate and argon/nitrogen gas, a detailed description of the flow field is necessary. The temperature, in turn, affects the fluid properties and can alter the flow field.

### **Temperature gradient and cooling rate results**

The temperature and temperature gradient of a point in the middle of fabricated tracks are presented in [Figure 2](#) for both the use of argon and nitrogen gases during L-PBF. It may be observed that temperature and temperature gradient marginally decrease when shielding gas is

changed from Argon to Nitrogen. This is due to the change in the thermal properties of Argon and Nitrogen. The thermal conductivity of Argon is lower ( $\approx 40\%$ ) compared to that of Nitrogen. Additionally, the specific heat capacities (isochoric and isobaric) of Argon are almost half that of Nitrogen. Consequently, more thermal energy will be absorbed via convection when Nitrogen is used inside the L-PBF chamber. When Argon is used inside the chamber, the peak temperature is  $\sim 100\text{ }^\circ\text{C}$  higher than the condition in which Nitrogen is used. The peak temperature gradient when using Argon is  $11\%$  ( $4.3\text{ }^\circ\text{C}/\mu\text{m}$ ) higher than when using Nitrogen as the shielding gas.

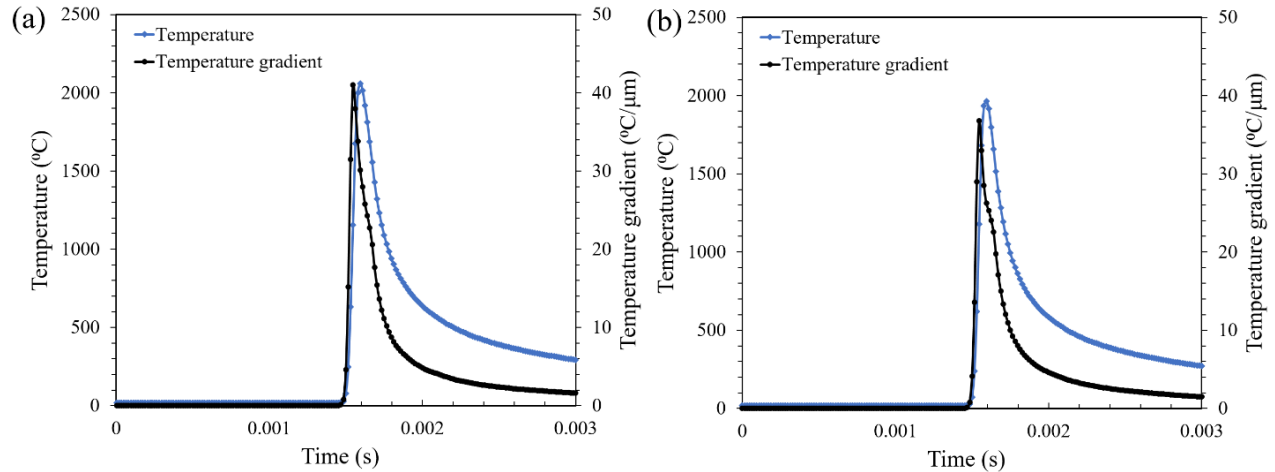


**Figure 2.** Temperature gradient at the middle of track under (a) Argon and (b) Nitrogen environments

It is observed in [Figure 3](#) that the cooling rate at the middle point of the track, is  $\approx 10\%$  higher when Nitrogen is used as the shielding gas. Like the previous case, the difference in thermal properties of Argon and Nitrogen causes the change in cooling rate. From the results, it is observed that convective heat transfer is more important when Nitrogen is used as a shielding gas compared to when Argon is used. This means that more energy will be dissipated by the environment when Nitrogen is used as the shielding gas.

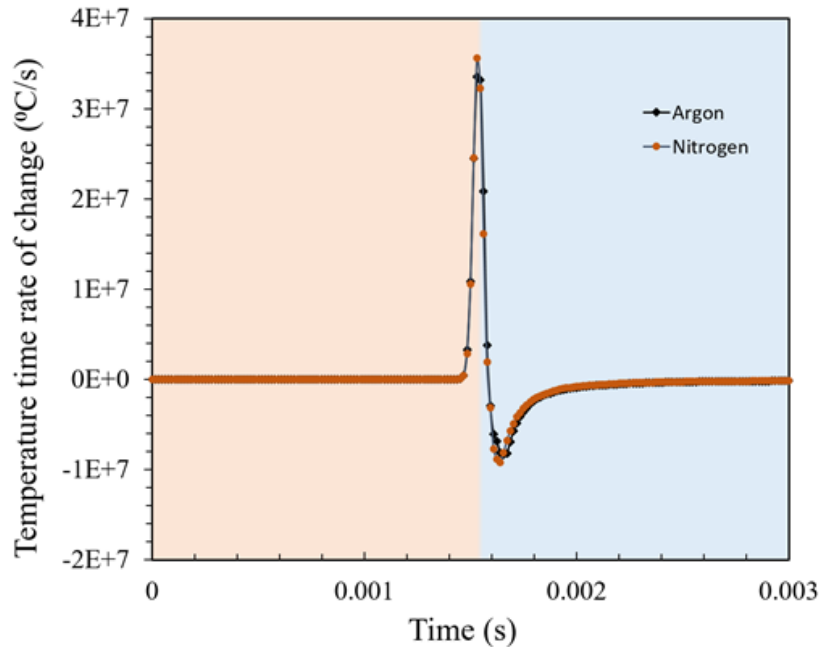


**Figure 3.** Cooling rate at the middle of track under Argon and Nitrogen atmosphere

### Experimental study

#### **Micro-hardness**

Figure 4 shows the micro-hardness results for various conditions. These are the mean values of multiple micro-indentation along the transverse plane, parallel to the building direction in the gage section area. In addition, the minimum and maximum micro-hardness value after the same heat treatment for the wrought material is specified by dashed lines for comparison. It is observed that the AB-Ar/N<sub>2</sub> condition has higher hardness with less deviation compare to the AB-Ar/Ar condition which shows that the microstructure is more homogenized when using Nitrogen as the shielding gas. This is attributed to the higher cooling rate under Nitrogen shielding gas which may not let the grains to grow as much as that under the Argon atmosphere. Accordingly, smaller grains with higher dislocation density can cause higher hardness which is consistent with the micro-hardness results. Interestingly, the hardness value for the HT-Ar/Ar is higher than the HT-Ar/N<sub>2</sub> condition. It has been reported that fabricating parts under Nitrogen gas stabilizes the austenite at room temperature, while the microstructure of fabricated specimens under Argon gas is martensitic. The precipitation hardening behavior has been reported to be more pronounced in martensitic microstructure [15]. Therefore, the micro-hardness of HT-Ar/Ar should be more than that corresponding to the HT-Ar/N<sub>2</sub> condition. In addition, it is clear that the hardness of AM specimens is in the same range for the wrought counterparts.

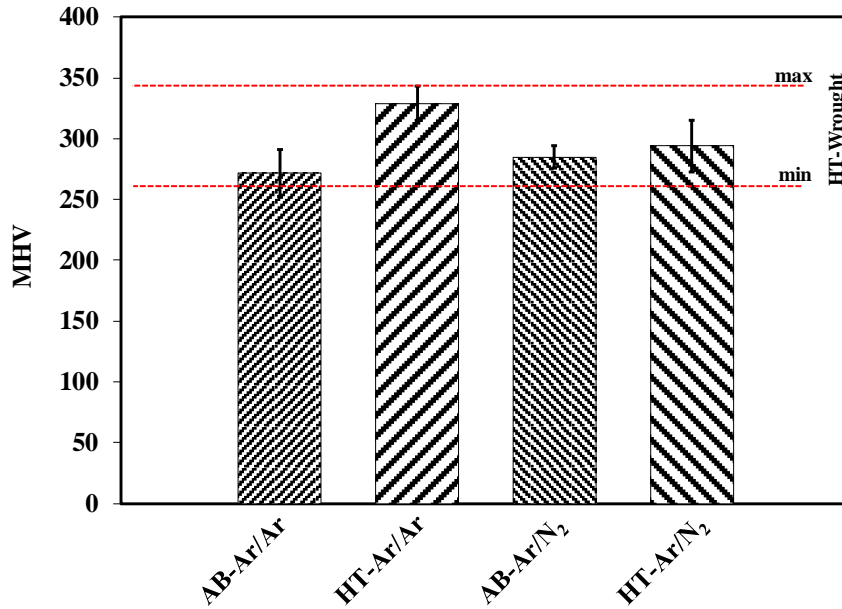


**Figure 4.** The micro-hardness results of specimens fabricated in Argon and Nitrogen L-PBF atmospheres for the as-built and heat-treated conditions

### Tensile properties

Figure 5 compares the monotonic mechanical behavior of specimens fabricated under Argon and Nitrogen atmosphere in the as-built and heat-treated conditions. Figure 3a shows the stress-strain curve up to the point the extensometer was removed. As it is observed, there is a minimal difference between Ar/Ar and Ar/N<sub>2</sub> conditions in the initial stages of deformation. Figure 3b represents the general tensile behavior of all conditions to failure and the corresponding details are summarized in Figure 3c. It may be seen that specimens responded similarly, irrespective of the shielding gas type. However, the Ar/N<sub>2</sub> specimens had insignificant higher strength and ductility (Figure 3b and c) in both as-built and heat-treated conditions. This is attributed to the higher cooling rates provided by the Nitrogen atmosphere which leads to finer microstructure. Moreover, the quantified microstructure characterization revealed that the aspect ratio of grains for the AB-Ar/N<sub>2</sub> condition is ~2 μm while it is ~2.4 μm for AB-Ar/Ar. Accordingly, there are more equiaxed grains for the Ar/N<sub>2</sub> condition which led to slightly higher specimen ductility than for the Ar/Ar condition.

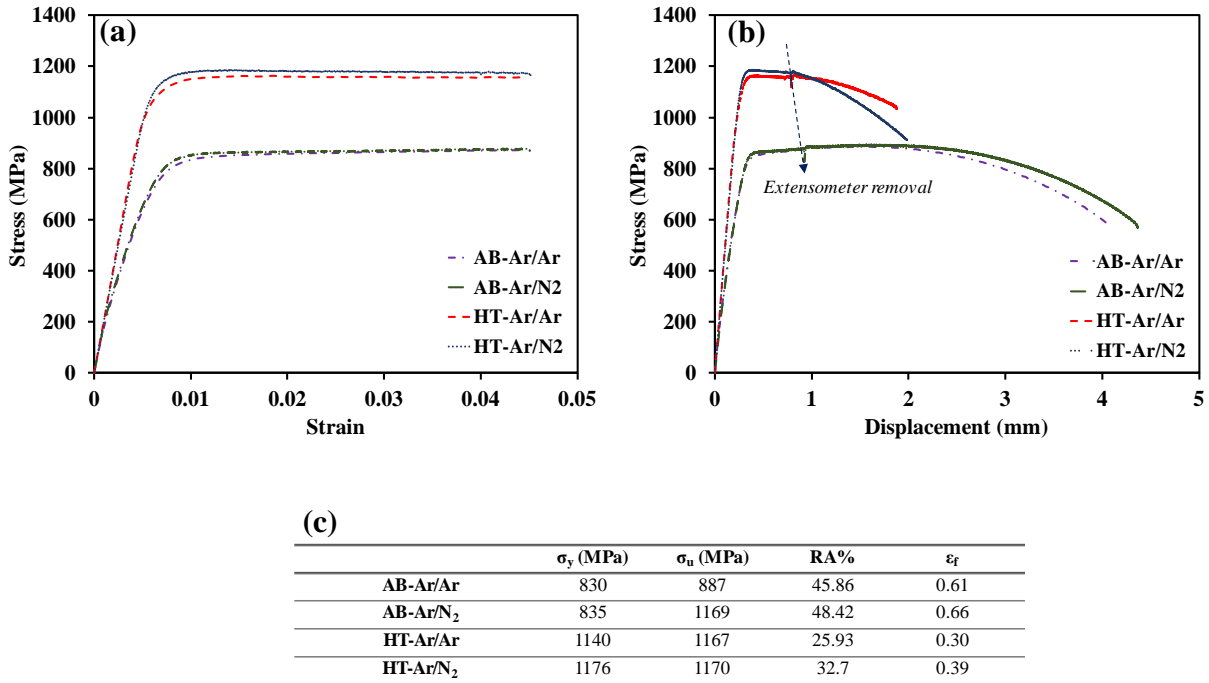


**Figure 5.** Tensile behavior of as-built and heat treated parts fabricated under Ar and N<sub>2</sub> shielding gases: (a) stress-strain curve up to 0.045 mm/mm where the extensometer was installed on the specimen (b) stress-displacement curve up to the failure and, (c) detailed tensile data

## Conclusions

The aim of this study was to investigate the effects of shielding gas type on the mechanical behavior of AM 17-4 PH SS. To this end, a numerical study was performed to obtain the temperature, temperature gradient and cooling rate of parts fabricated under Argon and Nitrogen shielding gases during L-PBF. Experimental investigations were carried out through micro-hardness testing and tensile tests to see the mechanical performance of fabricated parts under different shielding gases. The following conclusions can be made based upon the results:

1. Simulations showed that the Nitrogen atmosphere introduces slightly lower temperatures and temperature gradients along tracks while the cooling rate is higher than the Argon atmosphere. This is attributed to the higher thermal conductivity of Nitrogen gas ( $\approx 40\%$ ).
2. More energy should dissipate from the track to the environment when Nitrogen is used as the shielding gas. This is due to the higher cooling rate provided when using Nitrogen gas.
3. The hardness of as-built specimens fabricated under Nitrogen shielding gas is slightly higher than the fabricated specimens under Argon gas. This is attributed to the finer microstructure obtained due to the higher cooling rates provided while under Nitrogen atmosphere.
4. The HT-Ar/Ar specimens have higher hardness than HT-Ar/N<sub>2</sub> ones. This is due to the higher capability of precipitation hardening in the martensitic microstructure compared to the austenitic matrix as a result of fabricating under Argon atmosphere.

5. There is minimal variation in tensile behavior of all conditions. However, the specimens fabricated under Nitrogen atmosphere have slightly higher strength and ductility.

### **Acknowledgment**

This material is based upon the work supported by Naval Air Systems Command (NAVAIR)

### **References**

- [1] A. Yadollahi, N. Shamsaei, Additive manufacturing of fatigue resistant materials: Challenges and opportunities, *International Journal of Fatigue* 98 (2017) 14-31.
- [2] N. Shamsaei, A. Yadollahi, L. Bian, S.M. Thompson, An overview of Direct Laser Deposition for additive manufacturing; Part II: Mechanical behavior, process parameter optimization and control, *Additive Manufacturing* 8 (2015) 12-35.
- [3] A. Yadollahi, N. Shamsaei, S.M. Thompson, D.W. Seely, Effects of process time interval and heat treatment on the mechanical and microstructural properties of direct laser deposited 316L stainless steel, *Materials Science and Engineering: A* 644 (2015) 171-183.
- [4] R. Rashid, S.H. Masood, D. Ruan, S. Palanisamy, R.A. Rahman Rashid, M. Brandt, Effect of scan strategy on density and metallurgical properties of 17-4PH parts printed by Selective Laser Melting (SLM), *Journal of Materials Processing Technology* (2017).
- [5] M. Masoomi, J.W. Pegues, S.M. Thompson, N. Shamsaei, A numerical and experimental investigation of convective heat transfer during laser-powder bed fusion, *Additive Manufacturing* 22 (2018) 729-745.
- [6] P. Kah, J. Martikainen, Influence of shielding gases in the welding of metals, *International Journal of Advanced Manufacturing Technology* 64 (2013).
- [7] A. Ladewig, G. Schlick, M. Fisser, V. Schulze, U. Glatzel, Influence of the shielding gas flow on the removal of process by-products in the selective laser melting process, *Additive Manufacturing* 10 (2016) 1-9.
- [8] J. Sun, P. Nie, K. Feng, Z. Li, B. Guo, E. Jiang, The elimination of pores in laser welds of AISI 304 plate using different shielding gases, *Journal of Materials Processing Technology* 248 (2017) 56-63.
- [9] J.M. Kuk, K.C. Jang, D.G. Lee, I.S. Kim, Effects of temperature and shielding gas mixture on fatigue life of 5083 aluminum alloy, *Journal of Materials Processing Technology* 155-156 (2004) 1408-1414.
- [10] S. Zekovic, R. Dwivedi, R. Kovacevic, Thermo-structural finite element analysis of direct laser metal deposited thin-walled structures, *Proceedings SFF Symposium*,. Austin, TX, 2005.
- [11] H. Chung, S. Das, Numerical modeling of scanning laser-induced melting, vaporization and resolidification in metals subjected to step heat flux input, *International journal of heat and mass transfer* 47(19-20) (2004) 4153-4164.
- [12] M. Badrossamay, T. Childs, Further studies in selective laser melting of stainless and tool steel powders, *International Journal of Machine Tools and Manufacture* 47(5) (2007) 779-784.
- [13] J. Heigel, P. Michaleris, E. Reutzel, Thermo-mechanical model development and validation of directed energy deposition additive manufacturing of Ti-6Al-4V, *Additive manufacturing* 5 (2015) 9-19.
- [14] C. Schade, *Processing, Microstructures and Properties of a Dual Phase Precipitation-Hardening PM Stainless Steel*, 2010.

- [15] L.E. Murr, E. Martinez, J. Hernandez, S. Collins, K.N. Amato, S.M. Gaytan, P.W. Shindo, Microstructures and Properties of 17-4 PH Stainless Steel Fabricated by Selective Laser Melting, *Journal of Materials Research and Technology* 1(3) (2012) 167-177.
- [16] E.E.M. 12, Standard Test Method for Strain-Controlled Fatigue Testing, ASTM International (2012).
- [17] M. Masoomi, A. Yadollahi, S. M. Thompson, R. A. Winholtz, and J. Milner, "Assessment of Residual Stress in Selective Laser Melted 17-4 PH via Numerical Modeling and Neutron Diffraction," in MS&T Conference, 2016.
- [18] B. A. Younglove, "Thermophysical properties of fluids. I. Argon, ethylene, parahydrogen, Nitrogen, Nitrogen trifluoride, and oxygen," (1982).